Journal of Catalysis **199,** 19–29 (2001)
doi:10.1006/jcat.2000.3148, available online at http://www.idealibrary.com on IDEAL®

Hydrodesulfurization of Dibenzothiophene over Siliceous MCM-41-Supported Catalysts

I. Sulfided Co–Mo Catalysts

Anjie Wang,* Yao Wang,* Toshiaki Kabe,† Yongying Chen,* Atsushi Ishihara,† and Weihua Qian†

*State Key Laboratory of Fine Chemicals, Dalian University of Technology, 158 Zhongshan Road, Dalian 116012, People's Republic of China; and †Department of Applied Chemistry, Faculty of Technology, Tokyo University of Agriculture and Technology, 2-24-16 Nakacho, Koganei, Tokyo 184, Japan

Received June 14, 2000; revised December 11, 2000; accepted December 11, 2000; published online March 7, 2001

A deep hydrodesulfurization (HDS) catalyst, which was considerably active to desulfurize dibenzothiophene (DBT), was prepared by depositing Co–Mo species over siliceous MCM-41. The extremely high surface area of MCM-41 favors the dispersion of the active species, resulting in very high HDS activity. The optimal Co/Mo atomic ratio for this series of catalysts is 0.75, higher than the conventional γ-Al_2O_3-supported catalysts. This is attributed to the higher dispersion of the active species and more Co–Mo pairs generated on the surface of MCM-41. In the liquid product obtained at temperatures over 280°C, 70–80% BP was generated and its selectivity changed a little with increasing HDS reaction temperature. The selectivity of cyclohexylbenzene (CHB) decreased whereas the selectivity of benzene and cyclohexane increased when increasing the reaction temperature. It is shown that HDS of DBT over MCM-41-supported Co–Mo sulfides includes mainly three reaction pathways: hydrogenolysis, prehydrogenation followed by desulfurization, and hydrocracking of CHB. The hydrogenolysis of DBT, i.e., direct extraction of sulfur atom from DBT molecule, predominately progresses in the HDS reactions, while benzene mainly results from hydrocracking of CHB. ^{35}S isotope tracer investigation revealed that sulfur atoms retained on the surface could be released only by the introduction of a sulfur-containing compound, indicating that sulfur atom exchange between sulfur-containing compounds and the active sites is involved in the HDS reaction. A reaction mechanism for HDS is proposed, which is in accordance with the isotope tracer experiment results, the well-established rim–edge model, and the DFT calculations.

Key Words: **deep hydrodesulfurization; MCM-41; catalyst; mechanism.**

1. INTRODUCTION

The increasing concerns of global air environment have stimulated the demand for cleaner and cleaner engine fuels. In modern refinery, hydrotreating and hydrocracking have become key processes to meet this demand. Conventional catalysts used in the process include mainly Mo- or W-based catalysts supported by γ-Al_2O_3. They are active in converting thiophene and benzothiophenes, but not active enough to desulfurize efficiently the most refractory sulfur-containing polyaromatic compounds, e.g., dibenzothiophene (DBT) and its alkyl-substituted derivatives. Whitehurst *et al.* concluded, based on the composition of a typical gas oil and the first-order kinetics for hydrodesulfurization of different sulfur-containing compounds, that the reaction time will have to be increased by a factor of about 4 when using conventional catalysts to reduce the sulfur content from 2500 to 500 ppm (1). Thus, deep hydrodesulfurization becomes of great research interest, aiming at removing DBT and its derivatives.

Mesoporous MCM-41 has been the focus of much research interest since its discovery because it offers a uniform pore of 15 to 100 Å and a very high surface area (2). The unique properties of MCM-41 provide a potential for catalytic application to the bulky molecule involved reactions. The extremely high surface area favors a high dispersion of active species and is often conducible to high catalytic activity. The large pore channels may reduce pore diffusion limitation and allow the effective use of the active sites on the surface of the pore wall by the reactants. The MCM-41-supported catalysts have been developed for a variety of reactions (3), including hydrodesulfurization of petroleum fractions (4).

Shortly after the discovery of MCM-41, Corma *et al.* (4) used Al–MCM-41 to support Ni–Mo species in order to prepare catalysts for hydrocracking of vacuum gas oil. The prepared catalysts were investigated in terms of the activi ties of hydrodesulfurization (HDS), denitrogenation (HDN), and mild hydrocracking. They found that Al–MCM-41-supported catalysts were more active in HDS, HDN, and hydrocracking than those supported over USY or γ-Al_2O_3. Reddy *et al.* (5) supported Co–Mo and Ni–Mo over Al–MCM-41 to investigate the hydrodesulfurization of petroleum residues and atmospheric and vacuum

0021-9517/01 $35.00

residues. They also prepared γ-Al_2O_3-supported catalyst using the same procedure for comparison. The Al–MCM-41-supported catalyst was superior in HDS activity to its γ-Al_2O_3-supported counterpart, but not as active as the commercial catalyst. In the same group, Song and Reddy (6) also investigated the hydrodesulfurization of DBT over Co–Mo/Al–MCM-41 at both high and low metal loading. Co–Mo/Al–MCM-41 catalyst at normal metal loading level was less active in converting DBT than the γ-Al_2O_3-supported one at 350 or 375°C. However, The Al–MCM-41-supported catalyst at high metal loading was substantially more active than its γ-Al_2O_3-supported counterpart in DBT conversion. They concluded that sulfided Co–Mo/Al–MCM-41 catalysts are promising for deep hydrodesulfurization of distillate fuels under relatively mild conditions. It is interesting to note that all the research on MCM-41 type supports in HDS catalyst preparation has focused on Al–MCM-41, probably hoping that the strong acidity of the support may help to crack the polyaromatic sulfur-containing compounds so as to improve the HDS activity. Nevertheless, no great improvement in HDS activity has been achieved on this type of support.

Recently, Ramíre *et al.* (7) reported that strong acidity of the support (Al_2O_3 + MCM-41) was detrimental to the HDS activity of the catalysts. Only the weak and medium acids on the surface favor the formation of HDS active sites.

In the present study, the HDS of DBT over Co–Mo catalysts supported over siliceous MCM-41 has been investigated. And a radioisotope tracer method was used to trace the behavior of sulfur during HDS in order to elucidate the mechanism of HDS reaction.

2. METHODS

2.1. Materials

Both ammonium heptamolybdate tetrahydrate [$(NH_4)_6Mo_7O_{24}\cdot 4H_2O$] and cobalt nitrate hexahydrate [$Co(NO_3)_2\cdot 6H_2O$] were of commercial GR grade (Kishida Chemicals). Dibenzothiophene ([^{32}S]DBT) was the product of Acros Organics. Decalin was obtained from Kishida Chemicals and used as solvent without further purification. Hydrogen (99.99%) was supplied from Tohei Chemicals, and hydrogen sulfide in hydrogen (H_2S 5.0%) was from Takachio Chemicals. MCM-41, as the catalyst support, was prepared following the procedure reported in the previous paper (8). The preparation of the support included the hydrothermal reaction of a silica gel mixture of pH 10.5 at 130°C for 12 h and postsynthesis heat treatment at 600°C for 12 h in a N_2 flow followed by calcination in air at 540°C for 6 h. [^{35}S]DBT was synthesized by the following method: a commercial toluene solution of ^{35}S (total radioactivity, 1 mCi; Amersham Co., Ltd.) was mixed thoroughly with ^{32}S powder and then the solvent was evaporated at ambient temperature and dried for 24 h *in vacuo* to obtain ^{35}S-labeled sulfur. With the ^{35}S-labeled sulfur, [^{35}S]DBT was synthesized according to the method in the literature (9).

2.2. Catalysts

Co–Mo/MCM-41 catalysts were prepared in the following way. MCM-41 was impregnated with an aqueous solution of $(NH_4)_6Mo_7O_{24}\cdot 4H_2O$ and $Co(NO_3)_2\cdot 6H_2O$ for 12 h at room temperature, followed by the evaporation of solvent, an oven drying at 120°C for 5 h, and calcination in air at 450°C for 5 h. A 20 wt% MoO_3 loading level was chosen for preparing this series of catalysts. The content of cobalt was determined by varying the atomic ratio of Co/Mo in the range of 0–1.0. The catalysts were denoted as Co–Mo(x). The value in parentheses represents the atomic ratio of Co to Mo.

The X-ray diffraction (XRD) patterns of the MCM-41 and the supported catalysts were measured on a Rigaku RAD-2X diffractometer using nickel-filtered Cu$K\alpha$ radiation at 35 kV and 20 mA. Nitrogen adsorption measurements were performed using a Coulter SA 3100 adsorption analyzer, which reports adsorption isotherm, BET specific surface area, and pore volume automatically. The samples were outgassed for 4 h at 300°C before the adsorption.

The temperature programmed reduction (TPR) patterns of the Co–Mo catalysts were measured on a Chembet-3000 analyzer. Before the measurement, the sample has been treated in argon at 200°C for 2 h. A gas mixture of H_2 and Ar (5 vol% H_2 in argon) was used as the reacting agent. The patterns of the catalysts were measured from room temperature to 930°C at 10°C/min.

2.3. System and Procedure for HDS and Isotope Tracer

HDS of DBT was carried out in a fixed-bed stainless steel tubular reactor having a dimension of 8.0 mm in internal diameter. Catalysts were pelleted and then crashed and screened to 20–35 mesh. Catalyst particles (0.2 g) were diluted with quartz sand (30–50 mesh) to a constant volume of 1.5 cm^3 before being charged into the reactor. The HDS activities of the prepared catalysts were evaluated using a model fuel: 1 wt% DBT in decalin.

The catalysts were presulfided before HDS reaction by means of a mixture of H_2S/H_2 (5 vol% H_2S) at atmospheric pressure and 400°C for 3 h. After the presulfidation, the reactor was cooled to the HDS reaction temperature in H_2S/H_2 and then pressurized to 5.0 MPa by H_2. During the cooling period, the model fuel was fed into the reactor to wet the catalyst bed by a high-pressure metering pump (Kyowa Seimitsu KHD-16). The reaction conditions for the HDS reaction were temperature, 260–380°C; total pressure, 5.0 MPa; H_2/feed ratio, 1200 Nm^3/m^3; and WHSV, 45 h^{-1}. The reaction products were

separated in a gas–liquid separator to collect the liquid products. The H_2S produced was absorbed by bubbling through a commercial basic scintillator solution (Carbsorb, Packard Co. Ltd.). Sampling of both liquid and gas products was started 3 h after the reaction conditions had been achieved. For each run, three to five pairs of the liquid and absorbed H_2S solution samples were collected at intervals of 20 min. The liquid products were analyzed by a gas chromatograph equipped with an FID detector (Shimazu 17A, Shimazu Co. Ltd.) using a commercial capillary column (DB-1).

For ^{35}S-labeled isotope radioactivity tracer experiments, radioactivities of the unreacted [^{35}S]DBT in liquid products and the [^{35}S]H_2S in the absorbed solution were measured using a liquid scintillation counter (Beckman LS-6500, Beckman Co., Ltd.) after adding proper scintillator solvent (Permaflour or Instafluor, Packard Japan Co. Ltd.) to each fraction. Literature is available for the liquid scintillation counting (10).

To investigate the effect of H_2S on the HDS activities *in situ*, a pulse tracer method was developed. A pulse injection system is inserted in the stream of H_2, as shown in Fig. 1. After the HDS conversion became constant, 5.4 ml of [^{35}S]H_2S was introduced into the reaction bed by a six-way valve. The [^{35}S]H_2S absorbed in the Carbsorb solution was collected every 15 min, and its radioactivity was determined as mentioned above.

2.4. Measurement of Catalyst Activity

The activities of HDS, hydrogenolysis (HGY), hydrogenation (HYG), and hydrocracking (HYC) were estimated by the analysis of the liquid products, based on the well-established reaction path network shown in Fig. 2 (6). In the present study, the detectable compounds in the liquid samples include biphenyl (BP), cyclohexylbenzene (CHB), benzene, cyclohexane, and a trace amount of tetrahydrodibenzothiophene (TH-DBT). The conversion of DBT represents the activity of HDS for the catalysts, and the selectivity of BP is a measure of DBT hydrogenolysis. Since the chromatographic peak of benzene and cyclohexane is difficult to deconvolute, the formation of CHB is used to describe hydrogenation of DBT while the total of benzene and cyclohexane is used to represent of the hydrocracking of DBT.

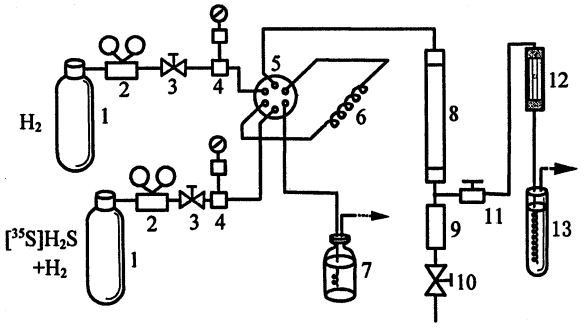

FIG. 1. Schematic diagram of the HDS reaction system with an isotope tracer pulse injection unit. 1, gas cylinder; 2, regulator; 3, stop valve; 4, pressure gauge; 5, six-way valve; 6, sampler loop; 7, trap bottle; 8, reactor; 9, gas–liquid separator; 10, stop valve; 11, needle valve; 12, flowmeter; 13, trap bottle.

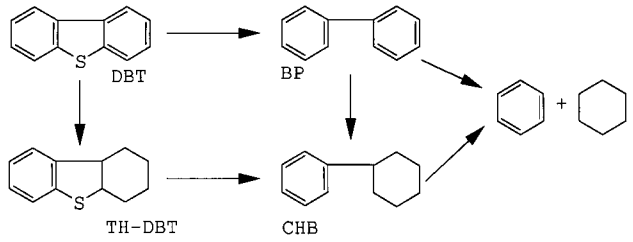

FIG. 2. Reaction path network for hydrodesulfurization of dibenzothiophene.

The rate constant of pseudo-first-order reaction of HDS of DBT, k_{HDS} (atom/nm$^2 \cdot$ s), was determined by (11)

$$k_{HDS} = \frac{-\ln(1-x) \cdot m \cdot F}{A},$$

where x is the conversion of DBT, m is the charge weight of the catalyst (g), F is the feed rate of DBT (atom/s), and A is the specific surface area (nm^2/g). Similarly, the rate constants of hydrogenolysis, hydrogenation, and hydrocracking of DBT are calculated as

$$k_{HYG} = k_{HDS} \cdot S_{BP}$$
$$k_{HYD} = k_{HDS} \cdot S_{CHB}$$
$$k_{HYC} = k_{HDS} \cdot S_{B+C}/2,$$

where S_{BP}, S_{CHB}, and S_{B+C} are selectivities of BP, CHB, and the total of benzene and cyclohexane, respectively.

To judge the limiting step involved in HDS reaction, the Weisz modulus (Φ) was used since the intrinsic reaction rate was not available. In the calculation, it was assumed that the HDS reaction was of first order with respect to DBT because H_2 was in large excess. The catalyst particles were approximately regarded as spherical, and the maximum particle size (0.84 mm) was used in the calculation. As the pore diffusion belongs to the Knudsen diffusion range for the mesoporous material, D_K was used as the mass transfer coefficient in the calculation.

3. RESULTS

3.1. Characterization of MCM-41 and Its Supported Catalysts

The X-ray diffraction patterns of the synthesized MCM-41 and the supported Co–Mo catalysts are shown in Fig. 3. It can be seen that there was a strong reflection at $2\theta = 1.92^\circ$, indicating that the mesostructure is well developed.

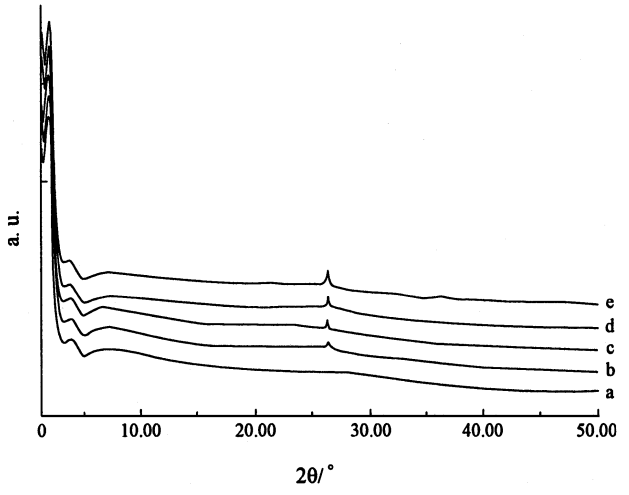

FIG. 3. XRD patterns of the synthesized siliceous MCM-41 and Co–Mo/MCM-41 catalysts. (a) Mo/MCM–41, (b) Co–Mo(0.25), (c) Co–Mo (0.50), (d) Co–Mo(0.75), (e) Co–Mo(1.00).

In the XRD patterns of the MCM-41-supported catalysts, no distinct reflection was observed except a small peak in the vicinity of $2\theta = 26^\circ$ which is assigned to $CoMoO_4$ crystal (Card No. 21-868). It is indicated that the CoO and MoO_3 species are highly dispersed on the surface of MCM-41.

The N_2 adsorption–desorption isotherm of the synthesized MCM-41 is shown in Fig. 4. It is a typical type IV isotherm of mesoporous materials. The N_2 adsorption amount increases sharply in the range of $P/P_0 = 0.3$–0.4. The sharp increase in uptake results from the capillary condensation of N_2, indicating that uniform mesopores are present in the siliceous MCM-41. From the isotherm, the structural parameters of the synthesized MCM-41 were evaluated: BET specific surface area, 1046 m^2/g; pore size, 46 Å; and pore volume, 1.00 cm^3/g.

The physical properties of the prepared catalysts are summarized in Table 1. It is shown that both BET specific surface area and pore volume of catalysts were reduced after depositing the metal species. The decreases in specific surface area and pore volume result partly from the density increase by depositing the metal species and partly from the pore blocking by the species. It can be seen that the pore volume decreases remarkably with increasing Co loading level, suggesting that pore blocking may be enhanced at high Co-loading levels.

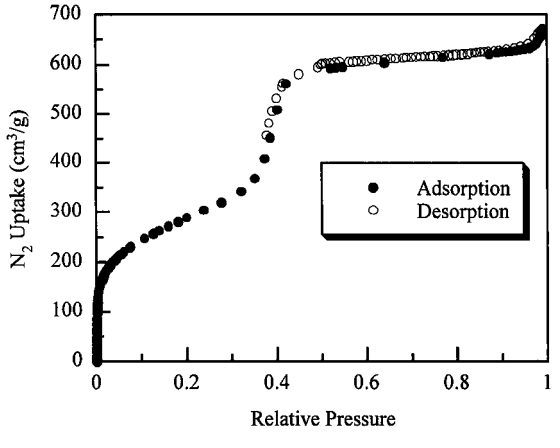

FIG. 4. N_2 adsorption–desorption isotherms of the siliceous MCM-41.

TABLE 1

Physical Properties of the Prepared Catalysts

Catalyst	BET surface (m^2/g)	Pore volume (cm^3/g)	Mo content ($atom/nm^2$)	Co content ($atom/nm^2$)
Mo/MCM-41	778	0.57	1.08	—
Co–Mo(0.25)	790	0.58	1.06	0.27
Co–Mo(0.50)	685	0.55	1.22	0.61
Co–Mo(0.75)	608	0.49	1.38	1.04
Co–Mo(1.00)	531	0.38	1.58	1.58

The TPR patterns of MCM-41 and its supported catalysts are illustrated in Fig. 5. The positions of the main TPR maxima are summarized in Table 2. It is indicated that the patterns are different from the normal Co–Mo/Al_2O_3 catalysts (12). The main maxima for Co–Mo/MCM-41 catalysts with high Co-loading correspond to the pattern of $CoMoO_4$, while a shoulder peak appears in the vicinity of 600°C. The TPR patterns of both Co/MCM-41 and Mo/MCM-41 are different from those of Co/Al_2O_3 and Mo/Al_2O_3. It is indicated that the interaction between the metal species and MCM-41 is quite different from that between the species and Al_2O_3.

3.2. Hydrodesulfurization of DBT

A model fuel containing 1 wt% DBT in decalin was used to investigate the HDS activities for Co–Mo sulfided catalysts supported over MCM-41. The main products are BP, CHB, benzene, and cyclohexane. In the temperature range of 260–380°C, the yield of TH-DBT decreased from trace to zero with increasing reaction temperature. Figure 6 shows the conversion of DBT over Co–Mo bimetallic catalysts supported over MCM-41 during hydrodesulfurization, compared with Co/MCM-41 (CoO, 20 wt%) and Mo/MCM-41

TABLE 2

Main Reduction Temperature in the TPR Patterns of MCM-41-Supported Catalysts

Catalyst	Main reduction temperature (K)
Co/MCM-41	773
Co–Mo(0.25)	817
Co–Mo(0.50)	828, 874
Co–Mo(0.75)	813, 862
Co–Mo(1.00)	849, 911, 1103
Mo/MCM-41	831

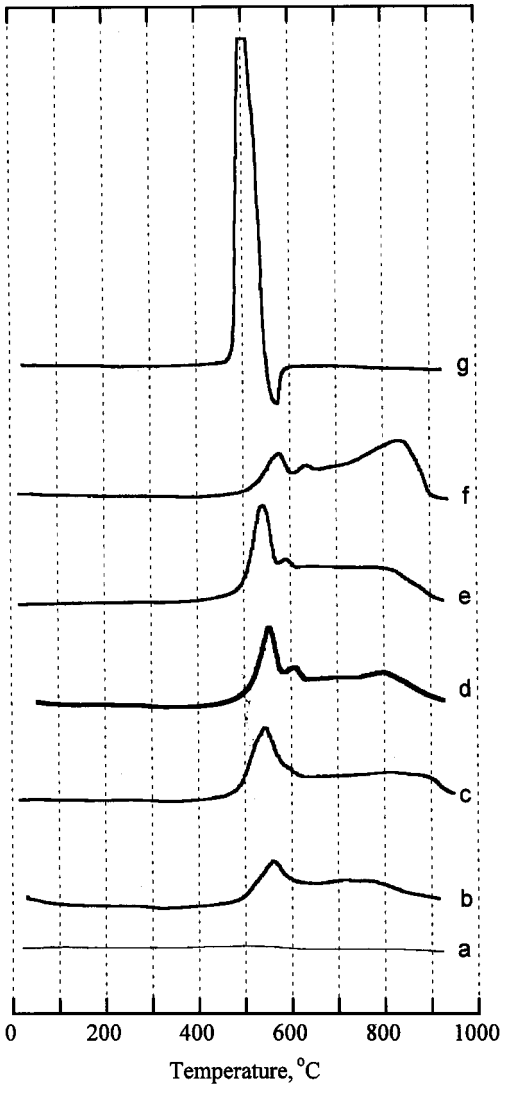

FIG. 5. TPR patterns of MCM-41 and its supported catalysts. (a) MCM-41, (b) Mo/MCM-41, (c) Co–Mo(0.25), (d) Co–Mo(0.50), (e) Co–Mo(0.75), (f) Co–Mo(1.00), (g) Co/MCM-41.

(MoO_3, 20 wt%). It is shown that all the Co–Mo catalysts showed very high activity for converting DBT into hydrocarbons, yielding almost complete conversion of DBT at temperatures over 320°C. Moreover, Mo/MCM-41 also showed relatively high HDS activity at high temperatures. It is shown that the Co–Mo(0.75)/MCM-41 catalyst exhibited the highest activity for DBT hydrodesulfurization. The optimal Co/Mo atomic ratio for MCM-41-supported catalysts is different from that for conventional γ -Al_2O_3-supported catalysts, which generally falls in the range of 0.2–0.5.

Figure 7 shows changes in HDS reaction rate with temperature for this series of catalysts. It is indicated that higher Co-loading favors the HDS reaction rate whereas HDS rate reaches a maximum at a Co/Mo atomic ratio of 0.75.

The variations of HDS selectivity with temperature for the Co–Mo catalysts are shown in Figs. 8a–8d. A small

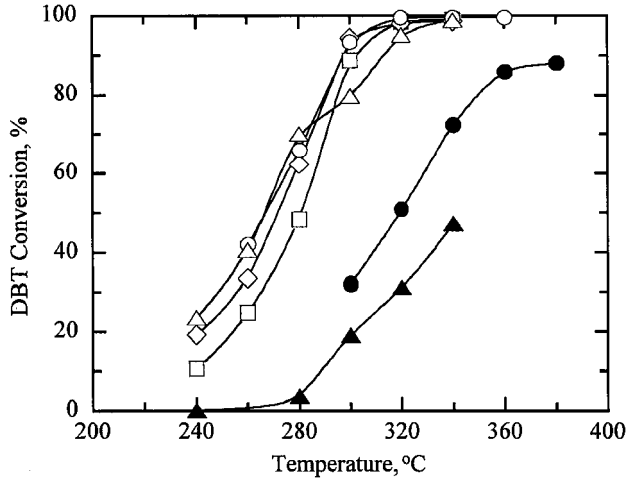

FIG. 6. Variation of DBT conversion with temperature during HDS over MCM-41-supported catalysts and a commercial deep HDS catalyst. (●) Mo, (□) Co–Mo(0.25), (◇) Co–Mo(0.50), (○) Co–Mo(0.75), (△) Co–Mo(1.00), (▲) Co.

part of DBT was converted into TH-DBT at temperatures below 280°C, but no TH-DBT was detected in the HDS reaction products obtained above 280°C. Since HDS of gas oil is generally carried out at temperatures >300°C and for ease of data treatment the selectivity data were curtailed to include only those in the temperature range of 280–360°C. As shown in the Fig. 8, the selectivity for BP formation changes a little for each catalyst and predominates in the liquid products (70–80%), indicating that HDS of DBT over MCM-41-supported Co–Mo catalysts mainly takes the route of hydrogenolysis. The selectivity of CHB decreases, whereas the selectivity of benzene and cyclohexane increases with increasing temperature, suggesting that high temperature favors the hydrocracking of CHB and that the

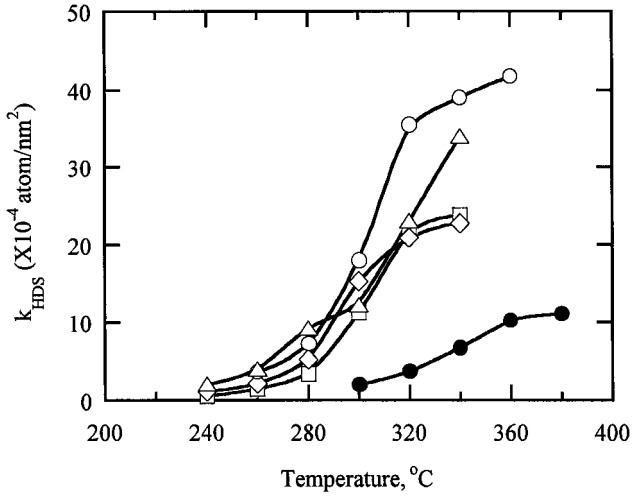

FIG. 7. HDS reaction rates vs reaction temperature for Co–Mo/MCM-41. (●) Mo, (□) Co–Mo(0.25), (◇) Co–Mo(0.50), (○) Co–Mo(0.75), (△) Co–Mo(1.00).

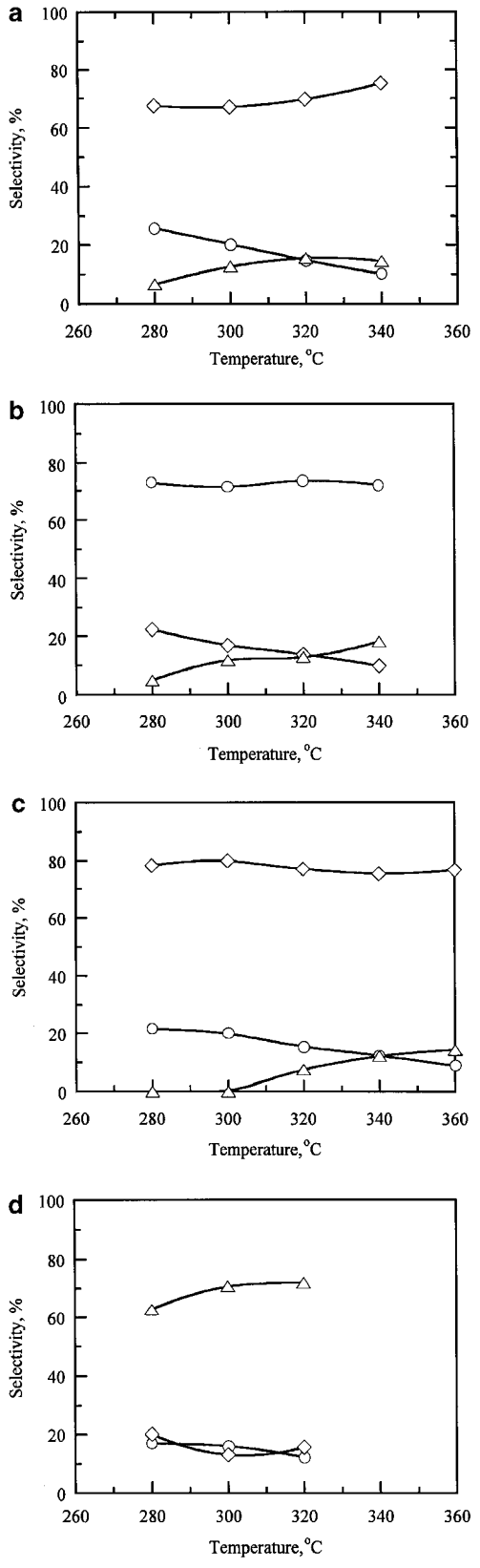

FIG. 8. Variation of selectivities for BP (◇), CHB (○), and benzene and cyclyhexane (△) with temperature during HDS of DBT. (a) Co–Mo(0.25), (b) Co–Mo(0.50), (c) Co–Mo(0.75), (d) Co–Mo(1.00).

TABLE 3

Reaction Constants for HDS, HYD, HYG, and HYC during HDS of DBT over Co–Mo Catalysts

Catalysts	Co–Mo (0.25)	Co–Mo (0.50)	Co–Mo (0.75)	Co–Mo (1.00)
300°C				
k_{HDS} ($\times 10^{-4}$ atom/nm^2 · s)	11.27	15.30	18.06	12.31
k_{HYD} ($\times 10^{-4}$ atom/nm^2 · s)	2.29	2.59	3.61	1.98
k_{HYG} ($\times 10^{-4}$ atom/nm^2 · s)	7.56	10.91	14.45	8.70
k_{HYC} ($\times 10^{-4}$ atom/nm^2 · s)	0.71	0.90	0.00	0.81
320°C				
k_{HDS} ($\times 10^{-4}$ atom/nm^2 · s)	21.72	20.89	35.60	23.05
k_{HYD} ($\times 10^{-4}$ atom/nm^2 · s)	3.21	2.88	5.48	2.83
k_{HYG} ($\times 10^{-4}$ atom/nm^2 · s)	16.35	15.33	27.41	16.59
k_{HYC} ($\times 10^{-4}$ atom/nm^2 · s)	1.69	1.34	1.36	1.81

hydrocracking of CHB mainly accounts for the formation of benzene and cyclohexane.

When the selectivities are plotted against HDS reaction conversion, the selectivities did not change markedly until the conversion exceeded 95%. At high conversions, the selectivity of BP changed a little while the selectivity of CHB decreased and the selectivity of benzene and cyclohexane increased with increase of conversion.

The reaction constants of HDS, hydrogenolysis, hydrogenation, and hydrocracking at temperatures of 300 and 320°C are summarized in Table 3. It is shown that hydrogenolysis reaction rate is the highest, one order of magnitude higher than other reactions.

The ratios of CHB selectivity to BP selectivity (S_{CHB}/S_{BP}) are plotted against HDS reaction temperature for MCM-41-supported Mo, Co, and Co–Mo catalysts, as shown in Fig. 9. It is shown that Mo/MCM-41 and Co/MCM-41 give

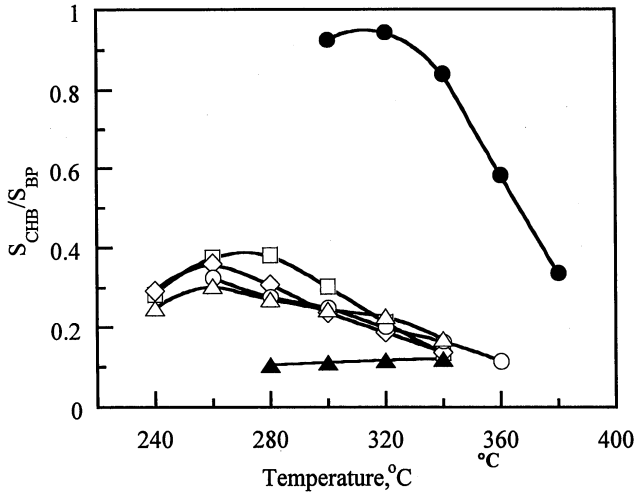

FIG. 9. S_{CHB}/S_{BP} vs reaction temperature for Mo, Co, and Co–Mo catalysts. (▲) Mo, (●) Co, (○) Co–Mo(0.25), (◇) Co–Mo(0.50), (△) Co–Mo(0.75), (□) Co–Mo(1.00).

the highest and the lowest S_{CHB}/S_{BP} ratio and the ratios for Co–Mo/MCM-41 catalysts fall between them.

The calculation of the Weisz modulus, Φ, for Co–Mo/MCM-41 catalysts in the temperature range of 240–360°C revealed that all the Weisz modula were below 0.04, indicating that intraparticle mass transfer is not the limiting step in HDS reaction in the reaction temperature range. Since the high space velocity during the reaction enhanced the external mass transfer around the particle, the reaction is not likely subject to mass transfer limitation. Consequently, the surface reaction should be the limiting step in the HDS reaction.

3.3. Sulfur Behavior during HDS by Isotope Tracer Method

The investigation of sulfur behavior during HDS of DBT was conducted over sulfided Co–Mo(0.50)/MCM-41 catalyst at 280°C and 5.0 MPa. Figure 10 shows a typical profile of radioactivity with reaction time during the HDS of DBT by the isotope tracer method. A decalin solution of 1 wt% [^{32}S]DBT was pumped into the reactor to run the HDS reaction. After the conversion of [^{32}S]DBT became constant, a flow of 1 wt% [^{35}S]DBT in decalin was introduced into the reactor to replace the [^{32}S]DBT solution. The radioactivity of the unreacted [^{35}S]DBT in the liquid product increased and approached a steady state immediately after the introduction, whereas there was a delay for the radioactivity of the released [^{35}S]H_2S to reach a steady state. After both the radioactivity of the unreacted [^{35}S]DBT and that of the released [^{35}S]H_2S became constant, a flow of decalin switched to replace the [^{35}S]DBT solution. Both the radioactivity of unreacted [^{35}S]DBT and that of released [^{35}S]H_2S decreased immediately. Little [^{35}S]DBT was detected during the period of purging with decalin and hydrogen, suggesting that there is no absorbed H_2S on the surface of the catalyst. After a long period of purging, a flow of 1 wt% [^{32}S]DBT solution was introduced again to replace decalin. No radioactivity change was detected in the liquid product, but a peak of ^{35}S radioactivity in the gas phase appeared in the form of [^{35}S]H_2S.

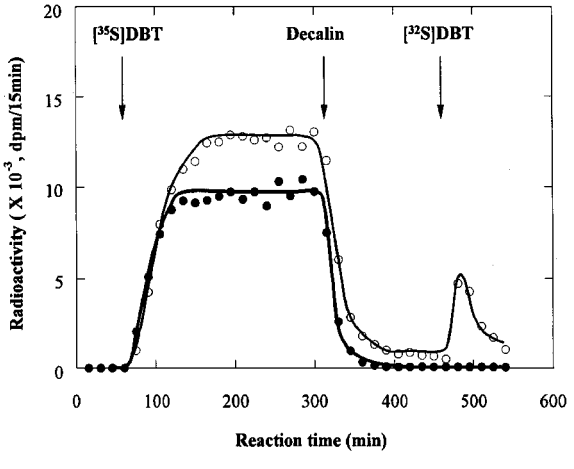

FIG. 10. Changes in radioactivities of unreacted [^{35}S]DBT (●) and released [^{35}S]H_2S (○) with reaction time.

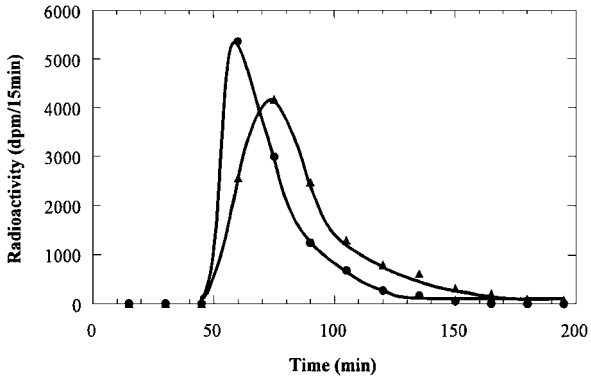

FIG. 11. Output profile of [^{35}S]H_2S with time after a pulse input during HDS reaction of DBT. (●) blank run, (▲) HDS.

The retarding effect of H_2S on HDS was reported by many researchers (13, 14). To investigate the behavior of the sulfur atom during HDS in the presence of H_2S, a pulse H_2S tracer method was developed to trace the dynamics of the sulfur atom. The experiment was conducted over the Co–Mo(0.50) catalyst at 320°C and 5.0 MPa. Figure 11 shows the comparison between the output profile of the blank run and that of the HDS run. For the blank run, there is a sharp peak in the output profile immediately after the introduction of [^{35}S]H_2S. For the HDS run, there was some delay for the radioactivity peak; moreover, the peak was broadened and was tailing.

4. DISCUSSIONS

4.1. Experimental Results

It is generally accepted that small cobalt sulfide species are located at the MoS_2 edges in the active phase (15). EXAFS measurements revealed that the Co sulfide species located at the MoS_2 edges differ locally in size and ordering (16). It is believed that only the Co–Mo–S structure is active in HDS. However, not all of the cobalt added to the formulation results in the formation of the unique Co–Mo–S species. As cobalt is added, it preferentially interacts with the edge of the MoS_2 crystallite surface, forming the desired active species. When all of the edges are covered, cobalt forms a separate phase of the stable sulfide Co_9S_8, which has no contribution to desulfurization. In other words, there is an optimal Co/Mo atomic ratio for every series of HDS catalysts.

Both the conversions of DBT and HDS rates for Co–Mo/MCM-41 catalysts indicated that the optimal Co/Mo

ratio is 0.75, higher than that of the conventional γ-Al_2O_3-supported catalysts. It is believed that a high dispersion of MoS_2 and the promoters on the surface of the supports is essential to form a monolayer or tiny Co–Mo–S crystallite structures so as to achieve a very high HDS activity (1). The XRD patterns of MCM-41-supported catalysts reveal that the active species are highly dispersed on the surface, even at a relatively high Mo loading. Since the support provides enough space to accommodate the Co–Mo pairs, higher HDS activity is obtained when the Co–Mo molar ratio is close to unit. Under such circumstances, the metal loading level becomes an important factor, since the loading will determine the population of the species pairs. Therefore, a high metal loading may be favored for such a high surface support.

The variation of BP selectivity with reaction temperature shows that HDS of DBT over MCM-41-supported Co–Mo catalysts mainly takes the route of hydrogenolysis. As can be seen in Fig. 9, Co/MCM-41 seems to accelerate the hydrogenolysis, and the introduction of Co to Mo-based catalysts enhances the direct extraction of sulfur atoms from the DBT molecule. It is assumed that Co sulfide desulfurizes by extracting sulfur atoms directly from the sulfur-containing molecules, perhaps due to its electronegativity higher than that of the Mo atom.

The variations of selectivities of CHB and of benzene and cyclohexane with temperature suggest that high temperature favors the hydrocracking of CHB and the hydrocracking of CHB mainly accounts for the formation of benzene. The analysis of bond dissociation energies for BP and CHB also supports the hypothesis that the hydrocracking of DBT mainly takes the route of CHB to benzene and cyclohexane. With lower dissociation energy (CHB, 389 kJ/mol; BP, 418 kJ/mol) (17), the C–C bond bridging the benzene ring and the cyclohexane ring in the CHB molecule is easier to be cleaved than that bridging the two benzene rings in the BP structure. Provided that benzene and cyclohexane are mainly produced via CHB cracking, the activation energies of the parallel reactions for BP and CHB formation might be of the same order of magnitude since their selectivities change little with the temperature.

The ^{35}S isotope tracer experiment (Fig. 10) shows that the sulfur atoms extracted from DBT molecules are not released directly, but accommodated on the surface. Since the ^{35}S accommodated on the catalyst cannot be released by H_2 and decalin purging for a couple of hours, the retained ^{35}S does not exit in the form of adsorbed H_2S on the surface. On the other hand, these sulfur atoms could be released by the introduction of new DBT molecules, indicating that sulfur atom exchange between DBT molecules and the surface of the catalyst may be involved during HDS of DBT and the sulfur atoms on the surface may serve as active sites.

Kabe *et al.* (18) reported similar results for the γ-Al_2O_3-supported Mo-based HDS catalysts. Moreover, they found that, in addition to sulfur, other heteroatoms with lone pairs such as nitrogen or oxygen also lead to the release of sulfur atoms on the active sites when introduced into the reaction system. If one considers the fact that Co–Mo nitrides are active in desulfurization (19) while Co–Mo sulfides are good catalysts for denitrogenation, it may be reasonable to assume that both sulfur and nitrogen atoms on the active sites are exchangeable and the exchange should be an important step in completing the catalytic circle. Nevertheless, the introduction of oxygen-containing molecules may considerably increase the period of the catalytic circle because oxygen atoms have stronger affinity to those transition metal cations. Presulfidation of the HDS catalyst prior to reaction provides evidence for this assumption because the presulfurization of Co–Mo oxides always takes several hours to completely replace oxygen atoms with sulfur atoms. In addition, Viljava *et al.* (20) recently studied the effect of alternating HDS and HDO (hydrodeoxygenation) cycles on the activity of a commercial presulfided Co–Mo/γ-Al_2O_3 catalyst by circling the feed between benzothiophene and phenol. They found that HDS conversion decreased after a HDO period, but the HDS activity of the catalyst was slowly recovered with time on sulfur-containing feed.

The results of pulse isotope tracer experiments showed that there was some delay of [^{35}S]H_2S output for the HDS run compared with the blank one. The profile for the HDS run is an additional result contributed by the residence of H_2S in the reactor and the stay of H_2S on the support. The difference suggests that the H_2S introduced during HDS not only adsorbs on the surface of the support but also is involved in interacting with the active site. H_2S, as one of the sulfur-containing molecules, competes with DBT in attacking the active site on the surface, so as to reduce the overall HDS reaction rate of DBT.

4.2. Mechanism of HDS over Mo-Based Catalysts

Despite the significant progress in HDS, many fundamental questions regarding the details of the catalytic cycle and the promoter action are still being debated. Many theories and models have been put forth and argued in the literature. Most of the models are based on the rim–edge model, in which hydrogenation sites are correlated with rim sites and hydrogenolysis sites are correlated with edge sites (1). According to the rim–edge model, the HDS selectivity results indicate that edge sites are predominant on the Co–Mo/MCM-41 catalyst, suggesting that the MoS_2 stacked lamellar crystals exist in very small crystals or in a monolayer structure. This conclusion is in accordance with the fact that the extremely high surface facilitates the high dispersion of the MoS_2 and CoS

species and the catalysts showed considerably high HDS activity.

In order to develop efficient deep HDS catalysts, much attention has been focused on the theoretical aspects of the active phase on the supports. It is commonly accepted that the vacancy on the surface acts as HDS active sites. Kabe *et al*. (11, 21, 22), based on the ^{35}S tracer results similar to those mentioned above, proposed that the S–C bonds in the DBT molecule were cleaved by the occupation of DBT on the vacancy and that H_2S formation leads to the regeneration of the new vacancy. Their model interpreted the phenomenon that the sulfur in DBT was not directly released as H_2S but was initially accommodated on the surface of the catalysts. However, the vacancy model could not account for the ^{35}S behavior shown in Fig. 8, because no $[^{35}S]H_2S$ was formed in the absence of DBT even in a hydrogen atmosphere while all the ^{35}S atoms accommodated on the surface were completely released as $[^{35}S]H_2S$ on introducing $[^{32}S]$DBT. Therefore, more detailed reaction steps need to be clarified.

Topsøe *et al*. (23) performed the DFT calculations in order to find the minimum energy configuration for the MoS_2 and Co–Mo–S structures on HDS catalysts. They concluded that quite large surface reconstruction/relaxation must take place during the catalytic cycle upon addition and removal of sulfur atoms. They have suggested that the many previous models based on static vacancy structures should be reconsidered (24). The DFT calculations (25) also revealed that the most favored positions of the Co promoter atoms are at the S edges, which is in accord with EXAFS results.

A hydrogenolysis catalytic circle during HDS over sulfided Co–Mo catalysts is proposed as shown in Scheme. 1. The mechanism briefly describes the possible reaction steps involved on the local site. It is assumed that gaseous hydrogen adsorbs dissociatively on the surface of catalysts and that the hydrogen species consumed in the reaction are supplemented by means of spillover on the surface (26).

During HDS over Co–Mo sulfided catalyst, the sulfur atom (S*) in the sulfur-containing molecules (H_2S, thiophene, benzothiophene, dibenzothiophene, etc.) tends to approach the Co atom at the edge site by hydrogen bonding. The Co–S bond, which bridges Co and Mo atoms, is weakened and then cleaved at the attack of a sulfur-containing molecule. With the cleavage of the Co–S bond, a SH group is formed by reacting with adsorbed hydrogen species, and a cationic Co is left on the surface. The two SH groups attached to the Mo atom are subsequently cleaved to release the sulfur atom on the active site as H_2S, and a double bond Mo=S is formed. By reacting with adsorbed hydrogen species, the double bond is broken to form a new SH group and a Mo cation. Both the cationic Mo and Co exert attractive forces on the sulfur atom in the sulfur-containing molecule, extracting the sulfur atom (S*) to bridge the Mo and Co atoms. Consequently, the chemical configuration on the catalyst surface resumes, and a new H_2 molecule from the gas phase adsorbs on the surface to fill the vacant adsorption site left. When a new sulfur-containing molecule approaches the active site, a new catalytic circle will begin.

It may be possible to replace the sulfur atom with a nitrogen atom to act as the active site. The prepared sulfided or nitrided Mo-based catalysts are active in both HDS and HDN of oil fractions. In other words, HDS and HDN share the same type of active sites during the hydrotreating process. However, the oxygen-containing

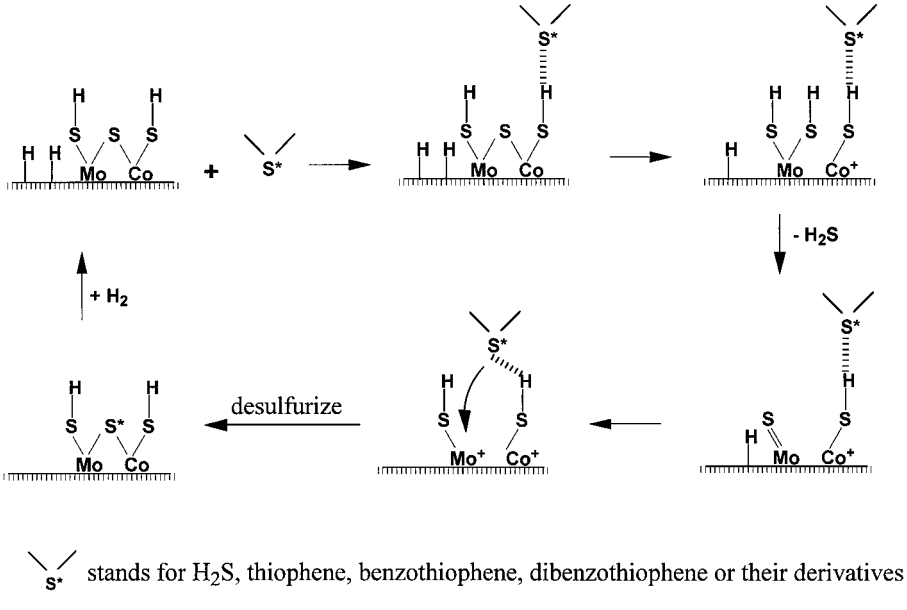

SCHEME 1. Mechanism of hydrodesulfurization of DBT over sulfided Co–Mo catalysts.

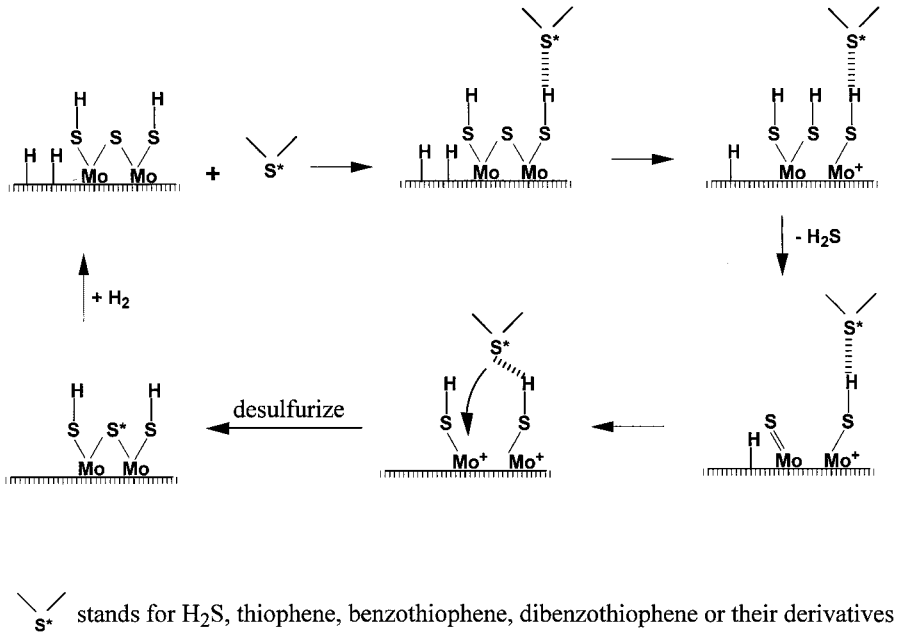

SCHEME 2. Mechanism of hydrodesulfurization of DBT over sulfided Mo catalysts.

compounds or gaseous oxygen are harmful to HDS and HDN, because the replacement of an oxygen atom by a sulfur atom is much more difficult on introducing sulfur-containing or nitrogen-containing feed.

It is worth noting that H_2S, like other sulfur-containing compounds, participates in the catalytic circle, as evidenced by the broadening and tailing of the output peak in the pulse tracer experiment during HDS. The competitive adsorption of H_2S results in a slowdown of the overall HDS reaction rate.

Similarly, the HDS reaction over Mo/MCM-41 catalyst takes the same steps. The cleavage and formation of bonds take place between the edged Mo atom and its neighboring Mo atom, as shown in Scheme 2. Since the Mo–S bond strength is higher than the Co–S bond strength (27), the Mo–S bond attached to the edged Mo atom is more difficultly cleaved than the Co–S bond. Consequently, the HDS reaction rate over Mo catalyst is lower than that over Co-promoted Mo catalysts. It seems that the cleavage of the Co–S bond or the Mo–S bond attached to the edged Mo atom might be the rate-limiting step.

5. CONCLUSION

In summary, siliceous MCM-41 is a promising support for preparing deep hydrodesulfurization catalysts. The optimal atomic ratio for Co–Mo/MCM-41 catalysts is 0.75, higher than that of the γ-Al_2O_3-supported catalysts. It is assumed that Co–Mo pairs have been created on the extremely high surface area, yielding considerably high activity for HDS of DBT.

In the liquid product obtained at temperatures over 280°C, 70–80% BP was generated and its selectivity changes a little with the increase in HDS reaction temperature. The selectivity of CHB decreases whereas the selectivity of benzene and cyclohexane increases when increasing the reaction temperature. It seems that HDS of DBT over MCM-41-supported Co–Mo sulfides includes mainly two parallel pathways: hydrogenolysis and hydrogenation followed by desulfurization. Benzene and cyclohexane in the liquid products are mainly from the hydrocracking of CHB. It is indicated that hydrogenolysis predominates in the HDS reactions of DBT.

^{35}S isotope tracer investigation revealed that sulfur atoms retained on the surface could be released only by the introduction of a sulfur-containing compound, indicating that sulfur atom exchange between sulfur-containing molecules and the active sites is involved in the HDS reaction. Accordingly, a reaction mechanism for HDS is proposed, which is in accordance with the isotope tracer results, the rim–edge model, and the DFT calculations.

ACKNOWLEDGMENTS

This research was partly supported by the Natural Science Foundation of China (20003002). The authors are grateful to Ms. D. Wang, Mr. X. Li, Mr. D. Han, Mr. S. Otsuki, Mr. H. Shirai, Mr. H. Sukuno, Mr. Putu, and Mr. Saito for their kind help with the research work. They also thank the Chinese and Japanese governments for financial support in carrying out the research program.

REFERENCES

1. Whitehurst, D. D., Isoda, T., and Mochida, I., *Adv. Catal.* **42**, 345 (1998).

2. Beck, J. S., Vartuli, J. C., Roth, W. J., Leonowicz, M. E., Kresge, C. T., Schmitt, K. D., Chu, C. T.-W., Olson, D. H., Sheppard, E. W., McCullen, S. B., Higgins, J. B., and Schlenker, J. L., *J. Am. Chem. Soc.* **114**, 10,834 (1992).
3. Ying, J. Y., Mehnert, C. P., and Wong, M. S., *Angew. Chem. Int. Ed.* **36**, 56 (1999).
4. Corma, A., Martínez, A., Martínez-Soria V., and Montón, J. B., *J. Catal.* **153**, 25 (1995).
5. Reddy, K. M., Wei, B., and Song, C., *Catal. Today* **43**(3–4), 261 (1998).
6. Song, C. S., and Reddy, K. M., *Appl. Catal. A* **176**(1), 1 (1999).
7. Ramíre, I., Contreras, R., Castillo, P., Klimova, T., Zárate, R., and Luna, R., *Appl. Catal. A: Gen.* **197**, 69 (2000).
8. Wang, A., and Kabe, T., *Chem. Commun.* **20**, 2067 (1999).
9. Gilman, H., and Jacoby, A. L., *J. Org. Chem.* **4**, 108 (1938).
10. Scheffer, B., Mangnus P. J., and Moulijn, J. A., *J. Catal.* **121**, 19 (1990).
11. Qian, W., Ishihara, A., Okoshi, Y., Nakakami, W., Godo, M., and Kabe, T., *J. Chem. Soc. Faraday Trans.* **93**(24), 4395 (1997).
12. Arnoldy, P., Franken, M. C., Scheffer, B., and Moulijn, J. A., *J. Catal.* **96**, 381 (1985).
13. Broderick, D. H., and Gates, B. C., *AIChE J.* **27**, 663 (1981).
14. Ledoux, M. J., Huu, C. P., Segura, Y., and Luck, F., *J. Catal.* **121**, 70 (1990).
15. Topsøe, N. Y., and Topsøe, H., *J. Catal* **84**, 386 (1983).
16. Bouwens, S. M. A. M., Van Zon, F. B. M., Wan Dijk, M. P., Van der Kraan, A. M., De Beer, V. H. J., Van Veen, J. A. R., and Koningsberger, D. C., *J. Catal.* **146**, 375 (1994).
17. Dean, J. A., "Handbook of Organic Chemistry," pp. 3–18. McGraw–Hill, New York, 1987.
18. Kabe, T., Qian, W., and Ishihara, A., *J. Phys. Chem.* **98**(3), 912 (1994).
19. Nagai, M., Koyama, H., Sakamoto, S., and Omi, S., *Stud. Surf. Sci. Catal.* **127**, 195 (1999).
20. Viljava, T., Komulainen, S., Selvam, T., and Krause, A., *Stud. Surf. Sci. Catal.* **127**, 145 (1999).
21. Kabe, T., Qian, W., and Ishihara, A., *J. Catal.* **149**, 171 (1994).
22. Qian, W., Ishihara, A., Wang, G., Tsuzuki, T., Godo, M., and Kabe, T., *J. Catal.* **170**, 286 (1997).
23. Topsøe, H., Knudsen, K. G., Byskov, L. S., Nørskov, J. K., and Clausen, B. S., *Stud. Surf. Sci. Catal.* **121**, 13 (1999).
24. Knudsen, K. G., Cooper, B. H., and Topsøe, H., *Appl. Catal. A: Gen.* **189**, 205 (1999).
25. Byskov, L. S., Nørskov, J. K., Clausen, B. S., and Topsøe, H., *J. Catal.* **187**, 109 (1999).
26. Hensen, E. J. M., Lardinois, H. J., de Beer, V. H. J., van Veen J. A. R., and van Santen, R. A., *J. Catal.* **187**, 95 (1999).
27. Byskov, L. S., Hammer, B., Nørskov, J. K., Clausen, B. S., and Topsøe, H., *Prepr. Am. Chem. Soc. Div. Pet. Chem* **42**(1), 113 (1997).